PHYSICAL REVIEW B **93**, 241202(R) (2016)

Topological semimetals with triply degenerate nodal points in θ-phase tantalum nitride

Hongming Weng,[1,2,*] Chen Fang,[1,†] Zhong Fang,[1,2] and Xi Dai[1,2]

[1]*Beijing National Laboratory for Condensed Matter Physics, and Institute of Physics, Chinese Academy of Sciences, Beijing 100190, China*

[2]*Collaborative Innovation Center of Quantum Matter, Beijing 100190, China*

(Received 29 April 2016; published 23 June 2016)

Using first-principles calculation and symmetry analysis, we propose that θ-TaN is a topological semimetal having a new type of point nodes, i.e., triply degenerate nodal points. Each node is a band crossing between degenerate and nondegenerate bands along the high-symmetry line in the Brillouin zone, and is protected by crystalline symmetries. Such new type of nodes will always generate singular touching points between different Fermi surfaces and three-dimensional spin texture around them. Breaking the crystalline symmetry by external magnetic field or strain leads to various topological phases. By studying the Landau levels under a small field along the *c* axis, we demonstrate that the system has a new quantum anomaly that we call "helical anomaly.'

DOI: 10.1103/PhysRevB.93.241202

I. INTRODUCTION

The discovery of topological semimetals (TSMs) is one of the major advancements in condensed matter physics within the last decade [1–3]. The type of TSM is determined according to the symmetry that protects the band crossing point near the Fermi energy and the effective Hamiltonian near that point. For example, a Dirac semimetal [4–6] is characterized by two bands with double degeneracy that cross near the Fermi level, and has to be protected by certain crystalline symmetry either at the high-symmetry point or along high-symmetry lines [7]. In contrast, the formation of a Weyl semimetal [8–19], which is characterized by the crossing of two nondegenerate bands at the Fermi level, does not require any protection from the crystalline symmetry other than lattice translation. In fact, the Weyl points in Weyl semimetals can be viewed as the "topological defects" in momentum space, which are stable under continuous deformation of the Hamiltonian [20,21]. Besides Dirac and Weyl semimetals, a nodal line semimetal is another type of TSM where two bands cross each other along a line in the Brillouin zone (BZ) [22–27].

Besides the above-mentioned Weyl, Dirac, and nodal line semimetals, there are other types of TSMs protected by nonsymmorphic space group symmetries, which are characterized by three-, six-, or eightfold degenerate points at the Fermi level and named as "new fermions" by Bradlyn *et al.* [28]. In the present Rapid Communication, a mechanism to generate "new fermions" is proposed with a realistic material θ-TaN in WC-type structure. In the band structure of θ-TaN [29] or similar materials [30–32], along a certain high-symmetry axis, both one- and two-dimensional representations are allowed, which makes it possible to generate band crossing between a doubly degenerate band and a nondegenerate band near the Fermi level at a triply degenerate nodal point (TDNP) [33,34]. This new type of three-component fermions can be viewed as the "intermediate species" between the four-component Dirac and the two-component Weyl fermions.

From another point of view, all the above listed TSMs can also be characterized by the topological features of the Fermi surface (FS) with the Fermi level near the band crossing points. For example, in Weyl semimetals the FS is nondegenerate with a nonzero Chern number [10,21], while in Dirac semimetals the FS is doubly degenerate and can be viewed as two FSs with opposite Chern numbers located on top of each other [5,21]. Compared to Weyl and Dirac semimetals, the FS in θ-TaN can be characterized by two nondegenerate FSs touching at one single point. Unlike the situation in the type-II Weyl semimetal state [19], where the FS touching appears only when the Fermi level is right at the Weyl point, in θ-TaN, the FS touching happens for a large range of chemical potential. Moreover a unique pattern of spin-momentum locking is found on the three-dimensional (3D) FS in θ-TaN, required by the crystalline symmetries.

For Weyl semimetals, the emergent "chiral anomaly" is related to the characteristic transport properties under an external magnetic field, i.e., the negative magnetoresistance along the direction of the magnetic field [35–37]. In the quantum-mechanical treatment for a single Weyl point under a magnetic field, the chiral anomaly manifests itself in the presence of a chiral zeroth Landau level propagating along the direction of the field. In the present Rapid Communication, we show that the Landau levels in θ-TaN exhibit a "helical anomaly," manifested by the presence of a pair of counterpropagating modes under an external field along the high-symmetry direction, the crossing of which is protected by the threefold rotation symmetry.

II. COMPUTATIONAL DETAILS

We have employed the software package OPENMX [38] for most of the first-principles calculations. Exchange-correlation potential is treated within the generalized gradient approximation (GGA) of Perdew-Burke-Ernzerhof type [39]. Spin-orbit coupling (SOC) is taken into account self-consistently. The sampling of the Brillouin zone in the self-consistent process is taken as the grid of $12 \times 12 \times 10$. The basis set for Ta and N is chosen as Ta9.0-$s2p2d2f1$ and N7.0-$s2p2d1$, respectively. The crystal structure and the stability of θ-TaN [29] has been recently revisited by Friedrich *et al.* [40] (Fig. 1). The experimental crystal structure is fully relaxed until the residual forces on each atom is less than 0.001 eV/Å. The possible underestimation of the band gap within GGA

*hmweng@iphy.ac.cn

†cfang@iphy.ac.cn

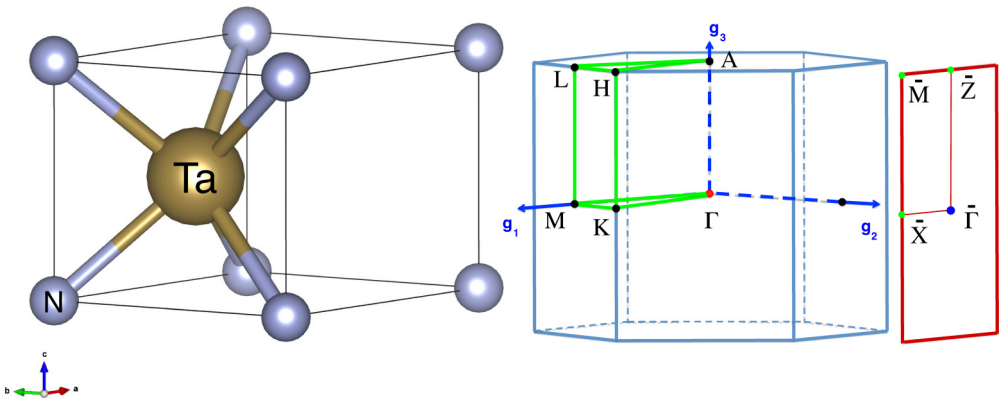

FIG. 1. (a) Crystal structure of θ-TaN. (b) 3D bulk BZ and projected (100) surface BZ with high-symmetry crystal momenta indicated.

is checked by nonlocal Heyd-Scuseria-Ernzerhof (HSE06) hybrid functional [41,42] calculation using the VASP software package [43,44]. To explore the surface states, we construct the maximally localized Wannier functions [45,46] for d orbitals of Ta by using OPENMX [38,47]. They are used as a basis set to build a tight-binding model for the semi-infinite system with surface in Green's function method [21,48].

III. RESULTS AND DISCUSSION

Crystal structure. The elements Ta and N can form many tantalum nitride phases [29,40]. θ-TaN can be synthesized at high pressure (2–10 GPa) within a proper high temperature range. After cooling and pressure relaxation, it can be stabilized and shows WC-type hexagonal crystal structure with space group $P\bar{6}m2$ (No. 187). Ta and N are at the $1d$ (1/3,2/3,1/2) and $1a$ (0,0,0) Wyckoff position, respectively. The experimental lattice constants are $a = b = 2.9333(1)$ Å and $c = 2.8844(2)$ Å [40]. The theoretical relaxed lattice constants are $a = b = 2.9697$ Å and $c = 2.9190$ Å, which are both overestimated by about 1.2% and used in the following calculations. NbN can also be crystallized in the same WC-type structure [30,31].

Band structure of θ-TaN. Figure 2(a) shows that θ-TaN is a semimetal with both hole and electron Fermi pockets. There is a band crossing along Γ-A. Without considering SOC, the fatted bands clearly show that the crossing bands are one nondegenerate band composed of a Ta d_{z^2} orbital and a double degenerate band from e_g orbitals (d_{xy} and $d_{x^2-y^2}$ orbitals). The crossing point is exactly threefold degenerate protected by the C_3 rotational symmetry on Γ-A. Such band crossing is due to the band inversion between the d_{z^2} state and the e_g states at A, which is similar to the case in Dirac semimetals Na_3Bi and Cd_3As_2 [5,6]. To overcome the possible overestimation of the band inversion within GGA, the hybrid functional HSE06 is used. It is found that this band inversion remains and furthermore, the hole pocket at momentum K within GGA disappears with the band maximum pushed down to lower than the Fermi level. Since Ta is heavy and the SOC cannot be ignored, we further calculate the band structure with SOC included self-consistently. Due to the lack of inversion symmetry, the spin splitting of bands at general momenta can be seen in Fig. 2(c). With SOC considered, the d_{z^2} orbital contains two states with $J_z = \pm 1/2$, where J_z is the total angular momentum. The two e_g orbitals contains four states with $J_z = \pm 1/2, \pm 3/2$. Due to the crystalline symmetries, the four $|J_z| = 1/2$ states form two doublets, while the two $J_z = \pm 3/2$ states are nondegenerate. (Here we remark that $3/2$ and $-3/2$ are equivalent because C_3 symmetry only preserves J_z up to a multiple of 3.) In the Brillouin zone, near A, these six states form six bands near the Fermi energy. Along Γ-A, due to the vertical mirror symmetry, the $|J_z| = 1/2$ bands are doubly degenerate, while $|J_z| = 3/2$ bands are nondegenerate; and due to C_3 symmetry, bands having different J_z cannot hybridize with each other [see Fig. 2(d)]. This leads to two protected triply degenerate nodal points (TDNPs) along Γ-A. We have also drawn the Fermi surfaces containing these two TDNPs by setting the chemical potential in between them around 110 meV. The two Fermi surfaces, in diamond and bell shapes, respectively, touch each other due to the double degeneracy of the $|J_z| = 1/2$ band. The bigger cylinderlike Fermi surface centering A is trivial since it does not enclose any band crossing points.

Some general remarks on the TDNP are due. First, the TDNPs appear in pairs due to the time-reversal symmetry. Second, for any Fermi level that is not far from the TDNP energy, the Fermi surface consists at least of two pockets touching at a point along Γ-A. Finally, while the TDNP itself is protected by C_3 and vertical mirror symmetry, a small perturbation breaking these crystalline symmetries cannot fully gap the system, because the Fermi surface has a finite size for any chemical potential. This is in contrast with Dirac semimetals protected by crystalline symmetries, where an infinitesimal symmetry-breaking perturbation can open a full gap at the Dirac point. This is also in contrast with type-II Weyl semimetals, where the touching of the electron and the hole pockets only appears when the Fermi level equals the energy of the Weyl point.

Band topology and surface states of θ-TaN. Although θ-TaN shows TDNPs along Γ-A and has both electron and hole Fermi pockets, its electronic structure within the $k_z = \pi$ and $k_z = 0$ plane can be looked at as two-dimensional (2D) insulators having time-reversal symmetry, which can give a well defined Z_2 topological invariant to identify the band topology. Since θ-TaN has no inversion symmetry, the Wilson loop method [21,48,49] is used to calculate this invariant. As shown in Fig. 3, the 2D electron bands in the $k_z = 0$ plane are trivial with the Z_2 invariant being 0, while those in the

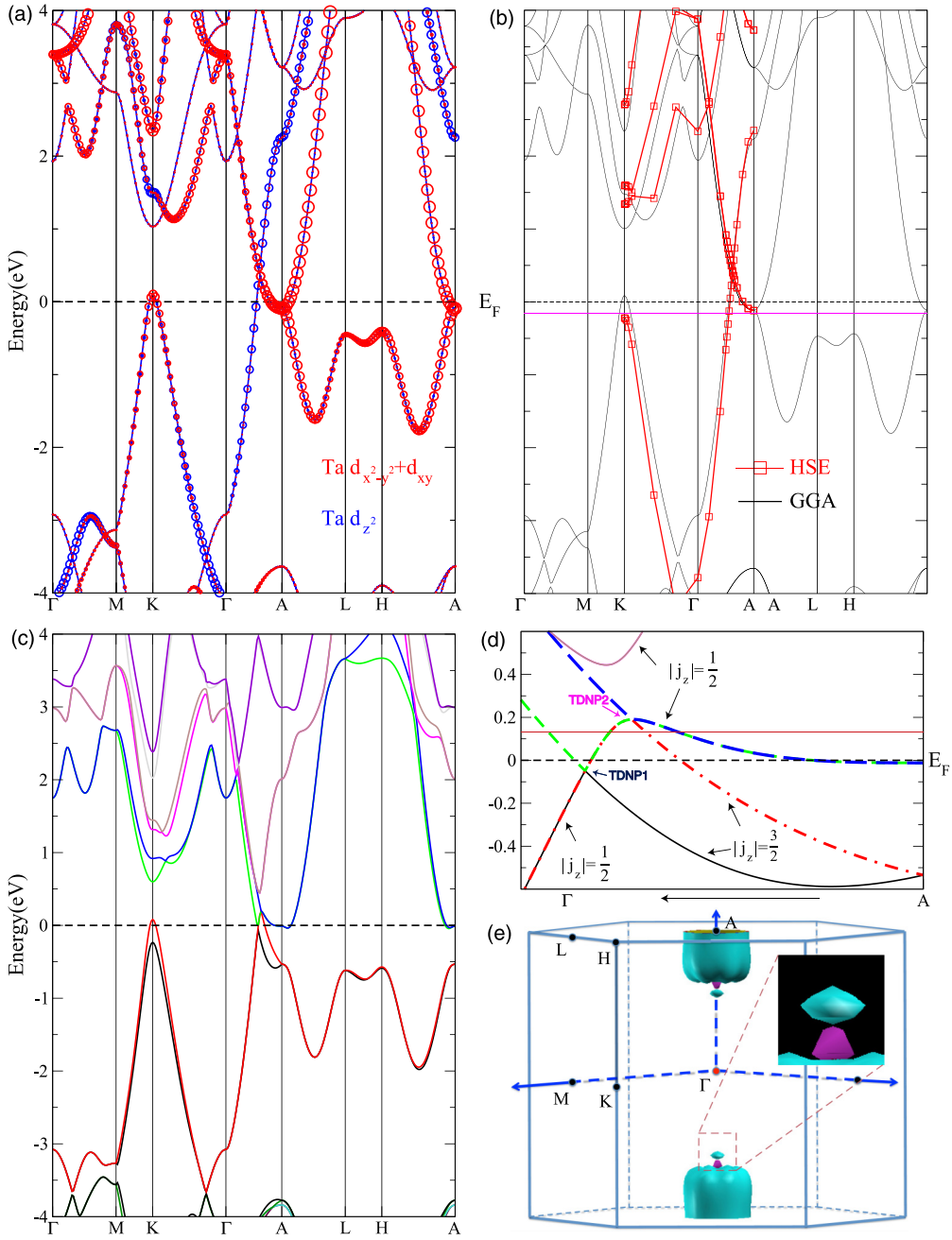

FIG. 2. Band structure of θ-TaN within GGA (a) with fatted bands projected onto Ta d_{z^2} and Ta e_g ($d_{x^2-y^2}$ and d_{xy}) orbitals and (b) in comparison with that calculated by using hybrid functional HSE06. (c) Band structure with SOC included. (d) Enlarged band structure along Γ-A in (c) around TDNP. (e) The Fermi surface with chemical potential at 110 meV within GGA+SOC.

$k_z = \pi$ plane have $Z_2 = 1$. These two planes will have edges along $\bar{\Gamma}$-$\bar{X}$ and $\bar{Z}$-$\bar{M}$, respectively, when cutting a plane [100] perpendicular to reciprocal lattice vectors $\mathbf{b_1}$ or $\mathbf{b_2}$ in Fig. 1(b). Due to the different Z_2 number in the $k_z = 0$ and $k_z = \pi$ planes, the number of crossings between edge states and any in-gap energy level should be even and odd along $\bar{\Gamma}$-$\bar{X}$ and $\bar{Z}$-$\bar{M}$, respectively, shown in Fig. 4. There is a Dirac conelike surface state centering $\bar{Z}$. The upper branch and lower branch connect to the conduction and valence bands, respectively, in both the $\bar{Z}$-$\bar{M}$ and the $\bar{Z}$-$\bar{\Gamma}$ directions. The surface states around $\bar{X}$ are trivial and both branches connect conduction states. As we have shown, the TDNPs are protected by both the C_3 axis and the vertical mirror plane, which are broken on a side surface such as the [100] surface; we hence do not expect features that are characteristic of the TDNP.

Now we consider the spin structure near the a TDNP. A TDNP in our system is a crossing between a $J_z = 3/2$ nondegenerate band and a $|J_z| = 1/2$ degenerate band, so near the crossing point, the dynamics of the electronic states are governed by the following three-band Hamiltonian:

$$H_3(\mathbf{q}) = \begin{bmatrix} u_{1/2}q_z & \lambda_1 q_+^2 & \lambda_2 q_+ \\ \lambda_1 q_-^2 & u_{1/2}q_z & \lambda_2 q_- \\ \lambda_2 q_- & \lambda_2 q_+ & u_{3/2}q_z \end{bmatrix}, \quad (1)$$

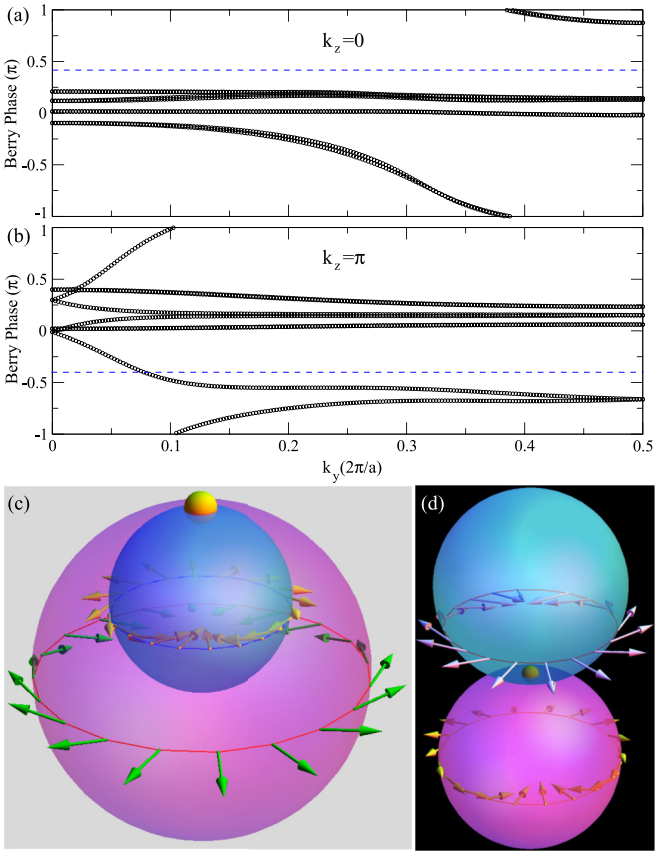

FIG. 3. The eigenvalues of the Wilson loops along the k_x axis at fixed k_y in the $k_z = 0$ (a) and $k_z = \pi$ (b) planes. The $k_z = \pi$ plane has a nontrivial Z_2 number of 1. (c) and (d) are the schematic plots of two tangent Fermi surface spheres enclosing two TDNPs with chemical potential sitting below (two hole pockets) and in-between (one electron and one hole pocket) the TDNPs, respectively. The spin winding number of 2 on each sphere is also shown.

where $\mathbf{q}$ is the momentum relative to the TDNP, $u_{1/2,3/2}$ are the velocities of the two bands along the z axis, $\lambda_{1,2}$ are real constants, and $q_\pm \equiv q_x \pm i q_y$. As we have shown, for any chemical potential near a TDNP, there are two carrier pockets touching each other at some point along Γ-A, where the Fermi level crosses the degenerate $|J_z| = 1/2$ band. Equation (1) implies that the degenerate band will split away from Γ-A, and the energy split is quadratic in $\mathbf{q}$. Equation (1) also reveals the spin structure of the Fermi surface: if we identify the $J_z = \pm 1/2$ state with a spin-up/down state, we find that along any horizontal loop on the Fermi surface, the spin winds exactly two rounds about the z axis, and that the two touching Fermi surfaces have opposite windings. This is a topologically robust feature of the Fermi surface near our TDNP. In Fig. 3, we plot the schematics of the Fermi surfaces for two chemical potentials near the TDNP, where there are two hole pockets [Fig. 3(c)] or one electron pocket and one hole pocket [Fig. 3(d)]; on each Fermi surface, we plot the typical spin structure along some latitude.

$\boldsymbol{k}\cdot\boldsymbol{p}$ model for θ-TaN. As discussed above, the low energy physics around the TDNPs and Fermi level are mostly determined by the bands spanned by degenerate $J_z = \pm\frac{1}{2}$ and nondegenerate $J_z = \pm\frac{3}{2}$ states. A $\boldsymbol{k}\cdot\boldsymbol{p}$ effective model can be constructed with these six states as the basis set. The momentum zero point is set at A.

Based on the orbital composition shown in Fig. 2(a), the most relevant orbitals are the following d orbitals of Ta: d_{z^2}, $d_{x^2-y^2}$, and d_{xy}. These orbitals plus spin degrees of freedom form the basis of the effective model: $\Psi = (d_{z^2\uparrow}, id_{z^2\downarrow}, id_{-2\downarrow}, d_{+2\uparrow}, id_{+2\downarrow}, d_{-2\uparrow})^T$, where $d_{\pm 2} \equiv d_{x^2-y^2} \pm i d_{xy}$. The derivation and the parameter fitting of the effective model is provided in the Supplemental Material [50], and in the main text, we briefly sketch the steps in its construction. First, we determine the little group of point A and how these basis states transform under the little group symmetries. Then we use the symmetry constraint

$$SH(\mathbf{q})S^{-1} = H(S\mathbf{q}) \tag{2}$$

to determine the form of $H(\mathbf{q})$ to a given order in $\mathbf{q}$, where S is the matrix representation of a little group symmetry, $\mathbf{q} \equiv \mathbf{k} - A$ is the momentum relative to A, and $S\mathbf{q}$ is $\mathbf{q}$ acted on by S. Finally, we use the dispersion from GGA to fit the parameters in the effective model.

An effective model helps us predict the effect of external fields. A uniform magnetic field induces a Zeeman field that couples to the spin degrees of freedom. The Zeeman field breaks time-reversal symmetry, but may preserve some crystal symmetry if applied along certain high-symmetry directions. For example, if $\mathbf{B} \parallel \hat{z}$, C_3 and M_z symmetries are preserved while T and M_y are broken. The TDNP point splits into two Weyl points with opposite monopole charges [see Fig. 5(a)]; if $\mathbf{B} \parallel \hat{y}$, M_y is preserved, while C_3 and $M_{y,z}$ are broken, and the TDNP splits into a nodal ring [see Fig. 5(b)].

Another external field we consider is the strain tensor, which may be induced by curving the substrate or by applying a local force field using an atomic force microscope. The strain tensor is parametrized by five components, namely, $\epsilon_{x^2-y^2,xy,xz,yz,z^2}$, among which $\epsilon_{xz,yz}$ do not couple into our model. In the other three components, ϵ_{z^2} do not break any symmetry, $\epsilon_{x^2-y^2}$ breaks C_3, and ϵ_{xy} breaks both C_3 and M_y symmetries. Therefore, either $\epsilon_{x^2-y^2}$ or ϵ_{xy} will split the three-band crossing point into line nodes and point nodes, respectively. (In the Supplemental Material, we explicitly write down the forms in which the Zeeman field and the strain tensor couple to the spin-orbital basis states.)

When a perturbation is added, the degenerate band of $|J_z| = 1/2$ will split, so the touching Fermi surfaces will also separate. The separate Fermi surfaces may or may not have a Chern number, depending on the nature of the symmetry-breaking perturbation. Also, we notice, in these examples, that independent of the form of perturbation, the three bands involved at a TDNP cannot be fully separated from each other in k space by these perturbations: there still remain nodal lines or Weyl points between these bands. This is similar to the robustness of a Weyl point against all types of perturbations.

Landau levels and helical anomaly. The large, anisotropic negative magnetoresistance observed in Weyl semimetals is considered an indirect proof for chiral anomaly, a hallmark of the Weyl fermions. This anomaly means that the total electric current is not conserved ($\partial_\mu J^\mu \neq 0$) on the quantum level, while the classical action remains invariant under the charge

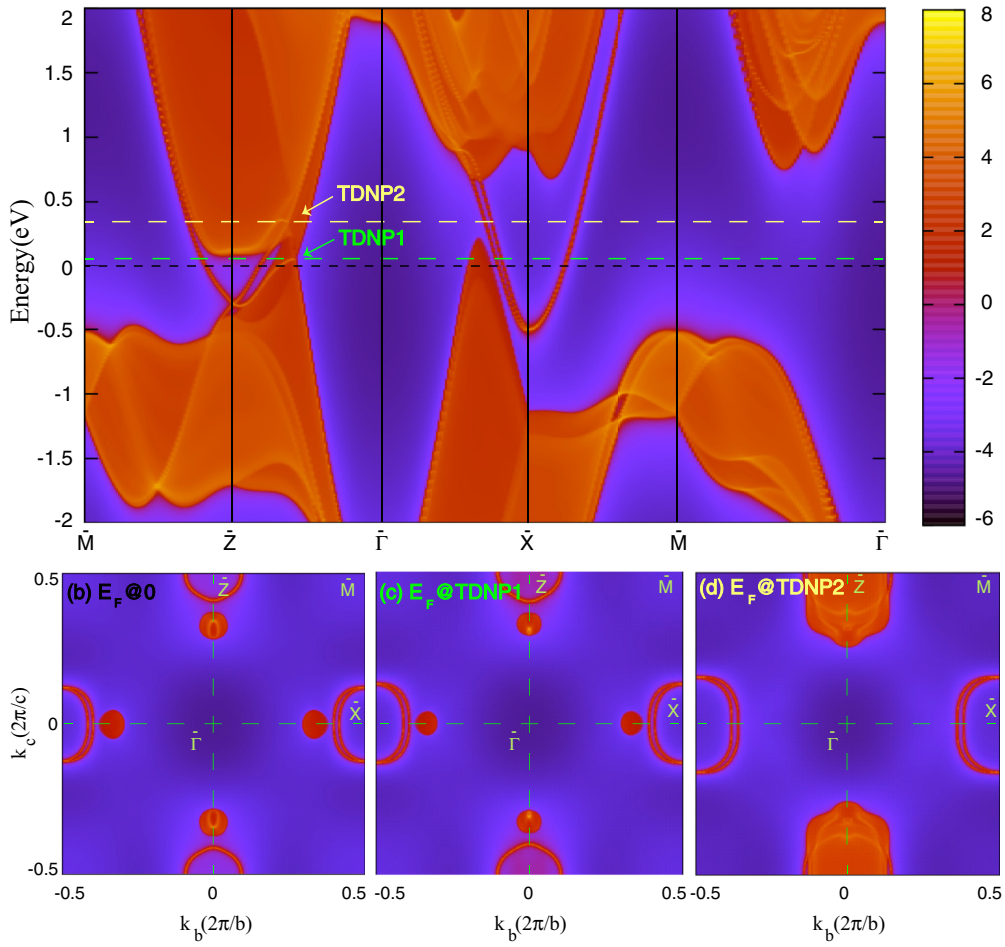

FIG. 4. TaN (100) surface state. (a) Band structure with weight projected onto one unit cell of the top surface. (b), (c), and (d) are Fermi surfaces with chemical potential at 0 eV, TDNP1, and TDNP2, respectively.

U(1) transform. The easiest way to see this is to consider the 3D Landau levels of Weyl fermions under a weak magnetic field along the z axis: the zeroth Landau levels at different k_z constitute one chiral mode going along the positive or negative z axis, depending on the monopole charge of the Weyl point. Therefore the total number of modes going along the $+z$ axis and the $-z$ axis become different, that is, the total current is nonvanishing. To check if our new semimetals have any type of quantum anomaly, we start with looking at the 3D Landau levels under a weak field.

On each side of A, there are two TDNPs close to each other, where two nondegenerate $3/2$ bands cross one degenerate $1/2$ band. The states near these triple crossing points can hence be described by a four-band model. In the Supplemental Material, we computed the Landau levels to the linear order of $k_{x,y}$ and field strength B and we find that there are always two counterpropagating modes along k_z. Since the rotation axis is unbroken if the field is along the z axis, one can still label these modes by their respective C_3 eigenvalues, finding that one mode has $C_3 = e^{-i\pi/3}$ and the other mode $C_3 = e^{i\pi/3}$, where $\pm$ depends on whether the field is along the $+z$ axis or the $-z$ axis. Since the two modes have different C_3 eigenvalues, their crossing is symmetry protected. In this case, the total charge current is zero as the two are counter propagating, but the net spin current is nonzero, because the two modes carry different J_z (or C_3 eigenvalues). These two zero modes can be compared to the pair of helical edge modes of a quantum spin Hall (QSH) state in several aspects. First, crossing of the two modes is protected (i.e., cannot be gapped) by rotation symmetry in our case, and by time-reversal symmetry in the case of the QSH state. Second, in both cases the two modes carry a net spin current. Finally, the backscattering between these modes is prohibited by rotation symmetry in our system and by time-reversal symmetry in the QSH state. Such similarities suggest the name "helical zeroth Landau level" (HZLL) for the two modes. The existence of HZLL under a small field indicates a new type of anomaly, termed "helical anomaly," that can be associated with this new type of semimetals. In terms of field theory, this anomaly means that while the classical action of effective theory for the Hamiltonian near the two TDNPs on one side of A is invariant under C_3 rotation, the quantum partition function is not. Again, similar to the chiral anomaly, when the whole BZ is taken into account, the anomaly vanishes, as one can see from the fact that the two triple crossings on the other side of A contribute a pair of helical modes carrying an opposite spin current. Therefore, the helical anomaly is physically relevant only as long as the intervalley scattering between the two sides of A is negligible.

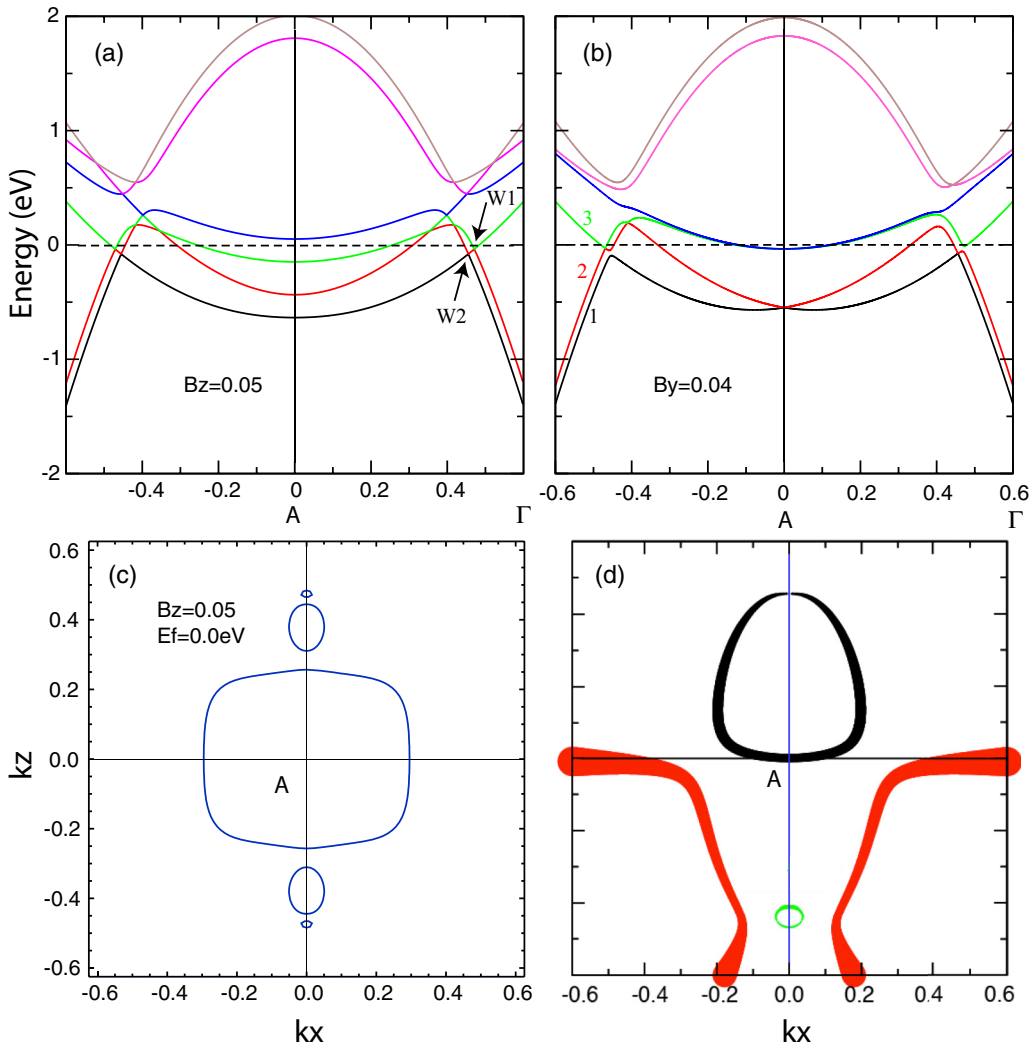

FIG. 5. Band structure along A-Γ. (a) Magnetic field is applied along the z direction. The Weyl nodes W1 and W2 with opposite chirality are indicated. (b) Magnetic field is applied along the y direction. The bands associated with TDNP are labeled as bands 1, 2, and 3. (c) The Fermi surface with chemical potential at 0 eV in (a). (d) The node lines formed by bands 1 and 2 (black and red) and bands 2 and 3 (green). The thickness of the node line represents the distance of nodal points to the Fermi level.

IV. DISCUSSION

The TDNP in θ-TaN should be compared with the recently proposed TDNP protected by nonsymmorphic symmetries. In the latter case, the TDNP appears at a high-symmetry point (BZ corner) and is pinned to that point, while in our case it is at a high-symmetry line and can move along the line by parameter tuning; in Ref. [28], at an ideal integer filling, the Fermi surface shrinks to a point, and by breaking some crystalline symmetry, the system can be fully gapped, while in our case the Fermi surface always has a finite size; in Ref. [28], the nonsymmorphic symmetries play a central role in the protection of the TDNP, while in θ-TaN the space group is symmorphic and the TDNP is protected by rotation and mirror symmetries.

Compared to other topological semimetals, the topology of the FS and its evolution under the external fields are the key features of the 'new fermion" state in θ-TaN. With the increase of the chemical potential, the FS evolves from hole-hole type to electron-hole type and finally to electron-electron type. Two Lifshitz transitions happen accordingly when the chemical potential hits two TDNPs. The existence of singular points on the FS will lead to interesting phenomena in transport, for example in the quantum oscillation behavior under a magnetic field. For each separate piece of FS, the quantum oscillation under a weak field can be explained nicely by the semiclassical theory with the phase of the quantum oscillation being determined fully by the accumulation of the Berry phase along the extremal orbits. For systems having a FS with touching points, the semiclassical orbits become undefined even at the low field due to the tunneling between two pieces of FS, a phenomenon known as the "magnetic breakdown" in quantum oscillation. Since the presence of the touching points on the FS is protected by the C_3 rotation symmetry, θ-TaN provides an ideal platform for the quantum transport studies for such systems.

V. CONCLUSIONS

In conclusion, the "new fermion" state with triply degenerate nodal points can be realized in θ-TaN. The appearance of the nodal point is protected by the rotation

symmetry and mirror symmetry, which allows both 2D and 1D representations along the Γ-A direction. Breaking these symmetries by the external fields will lead to either Weyl semimetal or nodal line semimetal phases. The Landau level calculation manifests the presence of a helical anomaly in θ-TaN. Finally, for an arbitrary Fermi level, our "new fermion" state hosts FSs that touch each other, leading to interesting transport properties, e.g., the possible magnetic breakdown in the quantum oscillation experiments.

Note added: Recently, we became aware of the following related studies [51,52].

ACKNOWLEDGMENTS

We acknowledge support from National Natural Science Foundation of China (Grants No. 11274359 and No. 11422428), the National 973 program of China (Grant No. 2013CB921700), and the "Strategic Priority Research Program (B)" of the Chinese Academy of Sciences (Grant No. XDB07020100). Part of the calculations were performed on TianHe-1(A), the National Supercomputer Center in Tianjin, China.

[1] H. Weng, X. Dai, and Z. Fang, Topological semimetals predicted from first-principles calculations, J. Phys.: Condens. Matter **28**, 303001 (2016).

[2] C.-K. Chiu, J. C. Y. Teo, A. P. Schnyder, and S. Ryu, Classification of topological quantum matter with symmetries, arXiv:1505.03535 [Rev. Mod. Phys. (to be published).

[3] A. Bansil, H. Lin, and T. Das, Colloquium: Topological band theory, arXiv:1603.03576 [Rev. Mod. Phys. (to be published).

[4] S. M. Young, S. Zaheer, J. C. Y. Teo, C. L. Kane, E. J. Mele, and A. M. Rappe, Dirac Semimetal in Three Dimensions, Phys. Rev. Lett. **108**, 140405 (2012).

[5] Z. Wang, Y. Sun, X.-Q. Chen, C. Franchini, G. Xu, H. Weng, X. Dai, and Z. Fang, Dirac semimetal and topological phase transitions in A_3Bi (A = Na, K, Rb), Phys. Rev. B **85**, 195320 (2012).

[6] Z. Wang, H. Weng, Q. Wu, X. Dai, and Z. Fang, Three-dimensional Dirac semimetal and quantum transport in Cd_3As_2, Phys. Rev. B **88**, 125427 (2013).

[7] B. J. Yang and N. Nagaosa, Classification of stable three-dimensional Dirac semimetals with nontrivial topology, Nat. Commun. **5**, 4898 (2014).

[8] S. Murakami, Phase transition between the quantum spin Hall and insulator phases in 3D: Emergence of a topological gapless phase, New J. Phys. **9**, 356 (2007).

[9] X. Wan, A. M. Turner, A. Vishwanath, and S. Y. Savrasov, Topological semimetal and Fermi-arc surface states in the electronic structure of pyrochlore iridates, Phys. Rev. B **83**, 205101 (2011).

[10] G. Xu, H. Weng, Z. Wang, X. Dai, and Z. Fang, Chern Semimetal and the Quantized Anomalous Hall Effect in $HgCr_2Se_4$, Phys. Rev. Lett. **107**, 186806 (2011).

[11] H. Weng, C. Fang, Z. Fang, B. A. Bernevig, and X. Dai, Weyl Semimetal Phase in Noncentrosymmetric Transition-Metal Monophosphides, Phys. Rev. X **5**, 011029 (2015).

[12] S. M. Huang, S. Y. Xu, I. Belopolski, C. C. Lee, G. Chang, B. K. Wang, N. Alidoust, G. Bian, M. Neupane, C. Zhang, S. Jia, A. Bansil, H. Lin, and M. Z. Hasan, A Weyl Fermion semimetal with surface Fermi arcs in the transition metal monopnictide TaAs class, Nat. Commun. **6**, 7373 (2014).

[13] L. Lu, Z. Wang, D. Ye, L. Ran, L. Fu, J. D. Joannopoulos, and M. Soljačić, Experimental observation of Weyl points, Science **349**, 622 (2015).

[14] B. Q. Lv, H. M. Weng, B. B. Fu, X. P. Wang, H. Miao, J. Ma, P. Richard, X. C. Huang, L. X. Zhao, G. F. Chen, Z. Fang, X. Dai, T. Qian, and H. Ding, Experimental Discovery of Weyl Semimetal TaAs, Phys. Rev. X **5**, 031013 (2015).

[15] B. Q. Lv, N. Xu, H. M. Weng, J. Z. Ma, P. Richard, X. C. Huang, L. X. Zhao, G. F. Chen, C. E. Matt, F. Bisti, V. N. Strocov, J. Mesot, Z. Fang, X. Dai, T. Qian, M. Shi, and H. Ding, Observation of Weyl nodes in TaAs, Nat. Phys. **11**, 724 (2015).

[16] S.-Y. Xu *et al.*, Discovery of a Weyl Fermion semimetal and topological Fermi arcs, Science **349**, 613 (2015).

[17] L. Yang, Z. Liu, Y. Sun, H. Peng, H. Yang, T. Zhang, B. Zhou, Y. Zhang, Y. Guo, M. Rahn, D. Prabhakaran, Z. Hussain, S.-K. Mo, C. Felser, B. Yan, and Y. Chen, Weyl semimetal phase in the non-centrosymmetric compound TaAs, Nat. Phys. **11**, 728 (2015).

[18] Y. Zhang, D. Bulmash, P. Hosur, A. C. Potter, and A. Vishwanath, Quantum oscillations from generic surface Fermi arcs and bulk chiral modes in Weyl semimetals, Sc. Rep. **6**, 23741 (2016).

[19] A. A. Soluyanov, D. Gresch, Z. Wang, Q. Wu, M. Troyer, X. Dai, and B. A. Bernevig, Type-II Weyl semimetals, Nature (London) **527**, 495 (2015).

[20] Z. Fang, N. Nagaosa, K. S. Takahashi, A. Asamitsu, R. Mathieu, T. Ogasawara, H. Yamada, M. Kawasaki, Y. Tokura, and K. Terakura, The anomalous Hall effect and magnetic monopoles in momentum space, Science **302**, 92 (2003).

[21] H. Weng, R. Yu, X. Hu, X. Dai, and Z. Fang, Quantum anomalous Hall effect and related topological electronic states, Adv. Phys. **64**, 227 (2015).

[22] A. A. Burkov, M. D. Hook, and Leon Balents, Topological nodal semimetals, Phys. Rev. B **84**, 235126 (2011).

[23] H. Weng, Y. Liang, Q Xu, R. Yu, Z. Fang, X. Dai, and Y. Kawazoe, Topological node-line semimetal in three-dimensional graphene networks, Phys. Rev. B **92**, 045108 (2015).

[24] M. Zeng, C. Fang, G. Chang, Y.-A. Chen, T. Hsieh, A. Bansil, H. Lin, and L. Fu, Topological semimetals and topological insulators in rare earth monopnictides, arXiv:1504.03492.

[25] R. Yu, H. Weng, Z. Fang, X. Dai, and X. Hu, Topological Node-Line Semimetal and Dirac Semimetal State in Antiperovskite Cu_3PdN, Phys. Rev. Lett. **115**, 036807 (2015).

[26] Y. Kim, B. J. Wieder, C. L. Kane, and A. M. Rappe, Dirac Line Nodes in Inversion-Symmetric Crystals, Phys. Rev. Lett. **115**, 036806 (2015).

[27] C. Fang, Y. Chen, H.-Y. Kee, and L. Fu, Topological nodal line semimetals with and without spin-orbital coupling, Phys. Rev. B **92**, 081201 (2015).

[28] B. Bradlyn, J. Cano, Z. Wang, M. G. Vergniory, C. Felser, R. J. Cava, and B. A. Bernevig, New fermions, arXiv:1603.03093.

[29] G. Brauer, E. Mohr, A. Neuhaus, and A. Skokan, θ-TaN, eine Hochdruckform von Tantalnitrid, Monatsh. Chem. **103**, 794 (1972).

[30] L. B. Litinskii, The band structure of hexagonal NbN, Solid State Commun. **71**, 299 (1989).

[31] L. B. Litinsky, On Fermi's surfaces of hexagonal carbides and nitrides, Solid State Commun. **75**, 1009 (1990).

[32] H. Weng, C. Fang, Z. Fang, and X. Dai, Co-existence of Weyl fermion and massless triply degenerate nodal points, arXiv:1605.05186

[33] S. Zaheer, S. M. Young, D. Cellucci, J. C. Y. Teo, C. L. Kane, E. J. Mele, and A. M. Rappe, Spin texture on the Fermi surface of tensile-strained HgTe, Phys. Rev. B **87**, 045202 (2013).

[34] G. W. Winkler, Q.-S. Wu, M. Troyer, P. Krogstrup, A. A. Soluyanov, Topological Phases in $InAs_{1-x}Sb_x$: From Novel Topological Semimetal to Majorana Wire, arXiv:1602.07001.

[35] D. T. Son and B. Z. Spivak, Chiral anomaly and classical negative magnetoresistance of Weyl metals, Phys. Rev. B **88**, 104412 (2013).

[36] X. Huang, L. Zhao, Y. Long, P. Wang, D. Chen, Z. Yang, H. Liang, M. Xue, H. Weng, Z. Fang, X. Dai, and G. Chen, Observation of the Chiral-Anomaly-Induced Negative Magnetoresistance in 3D Weyl Semimetal TaAs, Phys. Rev. X **5**, 031023 (2015).

[37] P. Hosur and X. Qi, Recent developments in transport phenomena in Weyl semimetals, C. R. Phys. **14**, 857 (2013).

[38] See http://www.openmx-square.org.

[39] J. Perdew, K. Burke, and M. Ernzerhof, Generalized Gradient Approximation Made Simple, Phys. Rev. Lett. **77**, 3865 (1996).

[40] A. Friedrich, W. Morgenroth, L. Bayarjargal, E. A. Juarez-Arellano, B. Winkler, and Z. Konpkov, In situ study of the high pressure high-temperature stability field of TaN and of the compressibilities of ϑ-TaN and TaON, High Press. Res. **33**, 633 (2013).

[41] J. Heyd, G. E. Scuseria, and M. Ernzerhof, Hybrid functionals based on a screened Coulomb potential, J. Chem. Phys. **118**, 8207 (2003).

[42] J. Heyd, G. E. Scuseria, and M. Ernzerhof, Erratum: "Hybrid functionals based on a screened Coulomb potential" [J. Chem. Phys. **118**, 8207 (2003)], J. Chem. Phys. **124**, 219906 (2006).

[43] G. Kresse and J. Furthmüller, Efficiency of *ab-initio* total energy calculations for metals and semiconductors using a plane-wave basis set, Comput. Mater. Sci. **6**, 15 (1996).

[44] G. Kresse and J. Furthmüller, Efficient iterative schemes for *ab initio* total-energy calculations using a plane-wave basis set, Phys. Rev. B **54**, 11169 (1996).

[45] N. Marzari and D. Vanderbilt, Maximally localized generalized Wannier functions for composite energy bands, Phys. Rev. B **56**, 12847 (1997).

[46] I. Souza, N. Marzari, and D. Vanderbilt, Maximally localized Wannier functions for entangled energy bands, Phys. Rev. B **65**, 035109 (2001).

[47] H. Weng, T. Ozaki, and K. Terakura, Revisiting magnetic coupling in transition-metal-benzene complexes with maximally localized Wannier functions, Phys. Rev. B **79**, 235118 (2009).

[48] H. Weng, X. Dai, and Z. Fang, Exploration and prediction of topological electronic materials based on first-principles calculations, MRS Bull. **39**, 849 (2014).

[49] R. Yu, X. L. Qi, A. Bernevig, Z. Fang, and X. Dai, Equivalent expression of Z_2 topological invariant for band insulators using the non-Abelian Berry connection, Phys. Rev. B **84**, 075119 (2011).

[50] See Supplemental Material at http://link.aps.org/supplemental/10.1103/PhysRevB.93.241202 for the construction of $\boldsymbol{k}\cdot\boldsymbol{p}$ effective model around A, the coupling of Zeeman field and train tensor to it, as well as its Landau levels.

[51] Z. Zhu, G. W. Winkler, Q. Wu, J. Li, and A. A. Soluyanov, Triple point topological metals, arXiv:1605.04653.

[52] G. Chang, S.-Y. Xu, S.-M. Huang, D. S. Sanchez, C.-H. Hsu, G. Bian, Z.-M. Yu, I. Belopolski, N. Alidoust, H. Zheng, T.-R. Chang, H.-T. Jeng, S. A. Yang, T. Neupert, H. Lin, and M. Z. Hasan, New fermions on the line in topological symmorphic metals, arXiv:1605.06831.